2013

Observations of Sharp Oxalate Reductions in Stratocumulus Clouds at Variable Altitudes: Organic Acid and Metal Measurements During the 2011 E-PEACE Campaign

Environmental Science & Technology

Article

pubs.acs.org/est

Observations of Sharp Oxalate Reductions in Stratocumulus Clouds at Variable Altitudes: Organic Acid and Metal Measurements During the 2011 E-PEACE Campaign

Armin Sorooshian,[†,‡,*] Zhen Wang,[†] Matthew M. Coggon,[§] Haflidi H. Jonsson,[⊥] and Barbara Ervens[∥,#]

[†]Chemical and Environmental Engineering, University of Arizona, Tucson, Arizona 85721, United States

[‡]Atmospheric Sciences, University of Arizona, Tucson, Arizona 85721, United States

[§]Department of Chemical Engineering, California Institute of Technology, Pasadena, California 91126, United States

[⊥]Center for Interdisciplinary Remotely Piloted Aircraft Studies, Naval Postgraduate School, Monterey, California 93943, United States

[∥]Cooperative Institute for Research in Environmental Sciences, University of Colorado, Boulder, Colorado 80309, United States

[#]Chemical Sciences Division, NOAA Earth System Research Laboratory, Boulder, Colorado 80309, United States

Supporting Information

ABSTRACT: This work examines organic acid and metal concentrations in northeastern Pacific Ocean stratocumulus cloudwater samples collected by the CIRPAS Twin Otter between July and August 2011. Correlations between a suite of various monocarboxylic and dicarboxylic acid concentrations are consistent with documented aqueous-phase mechanistic relationships leading up to oxalate production. Monocarboxylic and dicarboxylic acids exhibited contrasting spatial profiles reflecting their different sources; the former were higher in concentration near the continent due to fresh organic emissions. Concentrations of sea salt crustal tracer species, oxalate, and malonate were positively correlated with low-level wind speed suggesting that an important route for oxalate and malonate entry in cloudwater is via some combination of association with coarse particles and gaseous precursors emitted from the ocean surface. Three case flights show that oxalate (and no other organic acid) concentrations drop by nearly an order of magnitude relative to samples in the same vicinity. A consistent feature in these cases was an inverse relationship between oxalate and several metals (Fe, Mn, K, Na, Mg, Ca), especially Fe. By means of box model studies we show that the loss of oxalate due to the photolysis of iron oxalato complexes is likely a significant oxalate sink in the study region due to the ubiquity of oxalate precursors, clouds, and metal emissions from ships, the ocean, and continental sources.

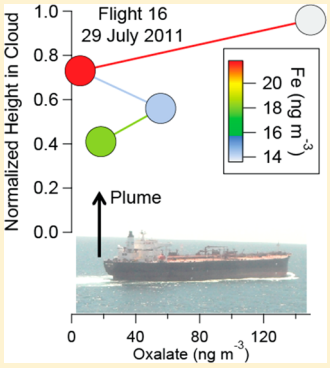

1. INTRODUCTION

An uncertainty in quantifying aerosol effects on visibility, clouds, climate, and public health is how to fully elucidate the sources and sinks of particle constituents. Models and measurements exhibit significant differences for both inorganic[1] and organic[2,3] concentrations in the aerosol phase, especially aloft.[4−6] Suggested explanations for discrepancies between models and measurements include incomplete knowledge of precursors and processes that convert organic gases into low-volatility products that contribute to secondary organic aerosol (SOA). One missing source in traditional models has been suggested to be an aqueous-phase production mechanism.[7−10] Studies in the past decade based on modeling,[2,9−16] laboratory-scale experiments,[17−25] and field measurements[26−34] suggest that SOA is generated via multiphase processes including the partitioning of soluble organic vapors into the aqueous phase and subsequent chemistry to produce lower-volatility species (e.g., organic acids) that remain in the aerosol phase upon subsequent evaporation of water.

Oxalic acid $(COOH)_2$, the most abundant dicarboxylic acid in tropospheric aerosol particles, is a tracer for aqueous phase-chemistry and has been shown to be especially abundant in the vicinity of clouds.[34−37] Measured oxalate concentrations in marine boundary layer clouds have been shown to be an order of magnitude less than predictions.[26] Oxalate losses include the direct oxidation by OH and the photolysis of Fe(III) oxalato complexes:

$$Fe(C_2O_4)_n^{3-2n} + h\nu \rightarrow Fe^{2+} + (n-1)C_2O_4^{2-} + CO_2 + CO_2^{-} (n = 2, 3) \quad \text{(R1)}$$

The latter process converts Fe(III) to a more soluble form, Fe(II).[38] Surface measurements in the Arctic indicate that

Received: March 22, 2013
Revised: June 12, 2013
Accepted: June 20, 2013
Published: June 20, 2013

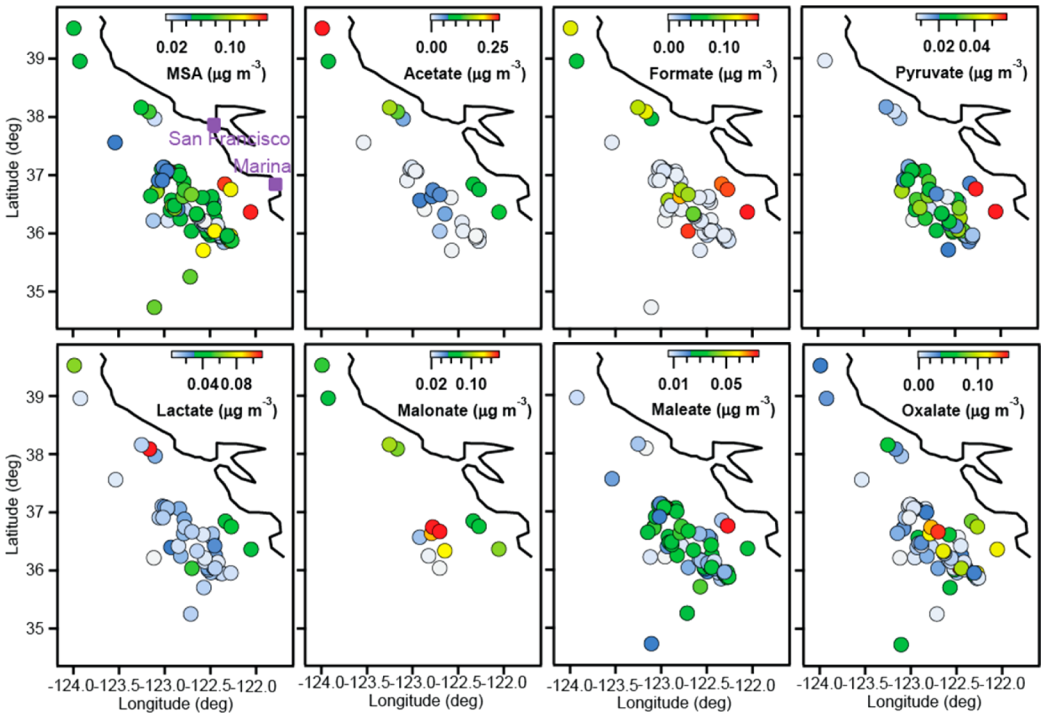

Figure 1. Spatial distribution of organic acid concentrations in E-PEACE cloudwater samples.

enhanced sunlight and Fe from dust degrade oxalate.[39] A critical data gap is the lack of vertically resolved measurements in clouds to address relationships between metals and organic acids.

The goal of this study is to examine the organic acid fraction of cloudwater in relationship to several metals using 81 cloudwater samples collected in northeastern Pacific Ocean stratocumulus clouds. Previous studies in this region focusing on oxalate production in clouds have neglected the simultaneous measurement of metals. This work is focused on (i) characterizing organic acid concentrations in relation to other major inorganic anions and metal cations, (ii) examining relationships between these cloudwater constituents, (iii) using three case flights to examine the sensitivity of organic acid concentrations to those of metals; and (iv) comparing the case flight data to box model results in order to explore the sensitivity of oxalate concentrations to iron redox cycling in cloudwater.

2. MATERIALS AND METHODS

2.1. Field Study Description. Thirty flights were conducted with the Center for Interdisciplinary Remotely-Piloted Aircraft Studies (CIRPAS) Twin Otter between July and August 2011 as part of the Eastern Pacific Emitted Aerosol Cloud Experiment (E-PEACE). The aircraft was based in Marina, California and the spatial extent of cloudwater sample collection is shown in Figure 1. Numerous aircraft field experiments have been conducted off the California coast in the last two decades due to the persistence of stratocumulus clouds and, in part, major aerosol perturbations due to ship emissions, which qualifies this region as a tailor-made venue to study aerosol-cloud interactions.[40−48] One of the central goals of E-PEACE was to examine how aerosol perturbations modify cloud properties and precipitation. In order to do this, a major emphasis was placed on flight paths targeting ships that produce significant particle number concentrations, the effect of which could be examined by the Twin Otter in cloud. The reader is referred to other work for a general overview of the E-PEACE campaign[48] and specific results related to aerosol physicochemical properties[49,50] and influence of ship emissions on cloud albedo.[51] A description of the relevant subset of Twin Otter instruments important for this work is provided below.

2.2. Cloud Water Measurements. Between one to six cloudwater samples of approximately 10−30 min duration were collected each flight, which typically lasted ∼4−4.5 h. Samples were obtained with a modified Mohnen slotted-rod cloudwater collector.[26,45,52] The collection efficiency of the collector increases with decreasing aircraft speed and has little correlation with drop diameter up to a mass mean diameter of approximately 35 μm;[53] the range of drop sizes encountered during E-PEACE are expected to have been sampled by the collector with variable size-dependent collection efficiencies. The drop-size dependent sampling efficiency and possible large drop shatter might bias the concentrations of metals, organics, and other solutes since their concentrations change with drop size (e.g., refs 54−57). Depending on biases in drop sizes measured, samples could be more enriched with species taken up via the gas phase (e.g., formic and acetic acids) as compared to those in scavenged particles.

Samples were collected by insertion of the collector upward through a port at the top of the aircraft when it was in cloud. Liquid samples traveled downward into detachable high-density polyethylene bottles. Cloud water samples were tested for pH immediately after collection, treated with chloroform to minimize biological processing of the samples, and then stored at a nominal 5 °C until laboratory analysis after the field campaign. Measurements of pH were conducted using an Oakton Model 110 pH meter calibrated with pH 4.01 and pH 7.00 buffer solutions.

A total of 81 cloudwater samples were divided into separate fractions to allow for both elemental and ionic composition analysis. A 500 μL fraction of each sample was analyzed with

ion chromatography (IC; Thermo Scientific Dionex ICS-5000 anion system with an AS11-HC 2 mm column) and for major inorganic and organic acid anions. Specific organic acids examined include three dicarboxylic acids (DCAs: oxalate, malonate, maleate), seven monocarboxylic acids (MCAs: acetate, formate, pyruvate, lactate, propionate, butyrate, glyoxylate), and methanesulfonate (MSA). IC analysis was conducted using a 38 min multistep gradient program with sodium hydroxide eluent (1 mM from 0 to 8 min, 1 mM to 30 mM from 8 to 28 min, 30 mM to 60 mM from 28 to 38 min). Background IC concentrations of blank cloudwater samples were subtracted from the measured sample concentrations. Background concentrations of species such as formic and acetic acids may represent an upper limit owing to soluble gases partitioning into the blank water samples. Species detection limits, calculated as three times the standard deviation of blanks, were less than 0.01 ppm for the IC species with errors less than 7%. Concentrations of glyoxylate are not reported owing to peak interference with a dominant chloride peak. As a result, only its presence in samples is reported.

Another fraction of each sample was analyzed with inductively coupled plasma mass spectrometry (ICP-MS). Forty μL of concentrated OPTIMA grade nitric acid was added to 1960 μL water sample fractions devoted to ICP-MS analysis. Twenty μL of a mixture containing 5 ppm aqueous Sc, Ge, In, and Bi internal standards (ICP-MS grade) were then added to each sample and the contents vortexted vigorously. Fifty-element semiquantitative measurements were then conducted on an Agilent 7700 Series ICP-MS in helium collision gas mode. As acidification of samples was not conducted immediately after collection, concentrations of specific constituents may be biased low in this work including iron and manganese.[37] A more extended discussion of cloudwater pH and IC/ICP-MS results will be addressed in separate work. Sodium (Na) measurements from ICP-MS are used to calculate non-sea salt sulfate concentrations (sea salt sulfate:sodium ~0.25[58]), hereinafter referred to as nss-sulfate.

2.3. Aerosol Chemical Measurements In and Out of Cloud. E-PEACE flights consisted of level legs at the following positions relative to the stratocumulus cloud deck: (i) below cloud; (ii) in cloud at usually three different altitudes (above bases, midcloud, and below tops); and (iii) above cloud tops. The Twin Otter was equipped with two inlets for sampling in or out of clouds. A subisokinetic total aerosol inlet was used out of cloud for clear-air aerosol characterization.[59] A new counterflow virtual impactor inlet (CVI[60]) was deployed for in-cloud sampling of cloud drop residual particle samples with a $D_{p,50}$ of 11 μm for the CVI flow-rate conditions and aircraft speed (~50 m s^{-1}) during E-PEACE. An Aerodyne compact time-of-flight aerosol mass spectrometer (C-ToF-AMS[61]) sampled downstream of these two inlets and quantified submicrometer mass concentrations of nonrefractory aerosol components (organics, sulfate, nitrate, chloride, ammonium). The C-ToF-AMS data used in this work include mass concentrations of total organics and one specific mass spectral marker representative of acid-like oxygenated organics (m/z 44; COO^+).[62,63]

Cloudwater species concentrations were converted to air-equivalent concentrations by multiplication with the average liquid water content (LWC) measured during the collection of individual cloudwater samples, which excludes out-of-cloud periods. To ensure the aircraft was in cloud, a threshold LWC value of 0.02 g m^{-3} was used. Liquid water content was measured with a PVM-100 probe.[64] Cloud drop size distributions were obtained using a cloud and aerosol spectrometer (CAS; D_p ~ 1−55 μm; Droplet Measurement Technologies, Inc.[65]). Sub- and above-cloud particle number concentrations were obtained with a condensation particle counter (CPC 3010; TSI Inc.) and a passive cavity aerosol spectrometer probe (PCASP; PMS Inc./DMT Inc.). The CPC and PCASP particle diameter size ranges are >10 nm and 0.1−2.6 μm, respectively. The upper size limit of the CPC is governed by the aircraft inlet, which has a roll-off in its collection efficiency starting at 3.5 μm and stabilizing at 5.5 μm at a value in excess of 60%.[59] An estimate of the subcloud aerosol not measured successfully by the C-ToF-AMS is obtained by comparing the PCASP volume concentration below 1 μm to the total volume concentration; the cumulative average (±standard deviation) subcloud ratio corresponding to areas where cloudwater samples were obtained was 41% ± 28%.

3. RESULTS AND DISCUSSIONS

3.1. Species Concentrations and Inter-relationships. The most abundant anion detected was chloride (Cl^-: 4.31 ± 5.12 μg m^{-3}), followed by nss-sulfate (nss-SO_4^{2-}: 1.04 ± 0.68 μg m^{-3}) and then nitrate (NO_3^-: 0.63 ± 0.63 μg m^{-3}) (Table 1). The organic acids exhibited average concentrations ≤0.09 μg m^{-3}. The average ratio of the total organic acid cloudwater concentrations (excluding MSA) to subcloud organic concentrations in submicrometer particles measured by the C-ToF-AMS was 16 ± 24% with a maximum value of 111%. Two reasons for why this ratio can exceed 100% include the following: (i) uptake and possible processing of organic acids or

Table 1. Summary of Cloud Water Constituent Concentrations in Air-Equivalent Units[a]

		n	min	max	average	σ
IC (μg m^{-3})	chloride	81	0.02	21.34	4.31	5.12
	NSS-sulfate	78	0.11	2.88	1.04	0.68
	nitrate	81	0.05	3.06	0.63	0.63
	malonate	14	0.02	0.15	0.09	0.04
	MSA	81	0.01	0.18	0.06	0.03
	acetate	30	0.00	0.27	0.05	0.06
	oxalate	69	0.00	0.15	0.03	0.04
	maleate	68	0.01	0.07	0.03	0.01
	pyruvate	53	0.01	0.06	0.02	0.01
	formate	55	0.00	0.16	0.03	0.05
	lactate	46	0.00	0.11	0.02	0.02
	propionate	7	0.00	0.02	0.01	0.01
	butyrate	8	0.00	0.01	0.01	0.00
	glyoxylate	7	NA	NA	NA	NA
ICP-MS (μg m^{-3})	Na	81	0.16	10.23	1.93	2.19
	Mg	81	0.81	1.38	0.26	0.29
	Si	47	0.00	4.39	0.19	0.80
	Ca	78	0.00	0.51	0.10	0.10
	K	70	0.00	0.34	0.07	0.07
ICP-MS (ng m^{-3})	Fe	61	0.21	21.76	3.52	4.10
	Zn	74	0.01	14.50	1.60	2.49
	V	81	0.03	3.12	0.66	0.67
	Mn	67	0.00	2.23	0.32	0.44
	Pb	50	0.00	0.32	0.05	0.06
	Cu	76	0.00	65.75	2.45	8.81

[a] σ represents standard deviation.

dx.doi.org/10.1021/es4012383 | Environ. Sci. Technol. 2013, 47, 7747−7756

Table 2. Correlation Matrix (r) for Cloud Water Constituent Concentrations[a]

	Cl^-	NSS SO_4^{2-}	NO_3^-	oxalate	malonate	maleate	MSA	acetate	formate	pyruvate	lactate	Ca	V	Mn	Fe	wind
Cl^-	1.00															
NSS SO_4^{2-}	0.36	1.00														
NO_3^-		0.90	1.00													
oxalate	0.53	0.49	0.38	1.00												
malonate	0.58	0.88	0.82	0.94	1.00											
maleate	0.33	0.38	0.27	0.26		1.00										
MSA	0.76	0.53	0.37	0.48		0.64	1.00									
acetate				0.60				1.00								
formate	0.36			0.56			0.41	0.88	1.00							
pyruvate		0.30				0.72	0.58	0.45	0.41	1.00						
Lactate						0.37	0.46	0.52	0.68	0.59	1.00					
Ca	0.95	0.44		0.56			0.74		0.40			1.00				
V	−0.26	0.69	0.84										1.00			
Mn		0.61	0.64		−0.70								0.53	1.00		
Fe		0.69	0.74										0.61	0.94	1.00	
Wind	0.35		−0.28	0.29	0.67						−0.32	0.30	−0.38	−0.37	−0.42	1.00

[a]Values shown coincide with statistical significance using a two-tailed student's t-test at 95% confidence. Propionate and butyrate are omitted due to limited sample numbers.

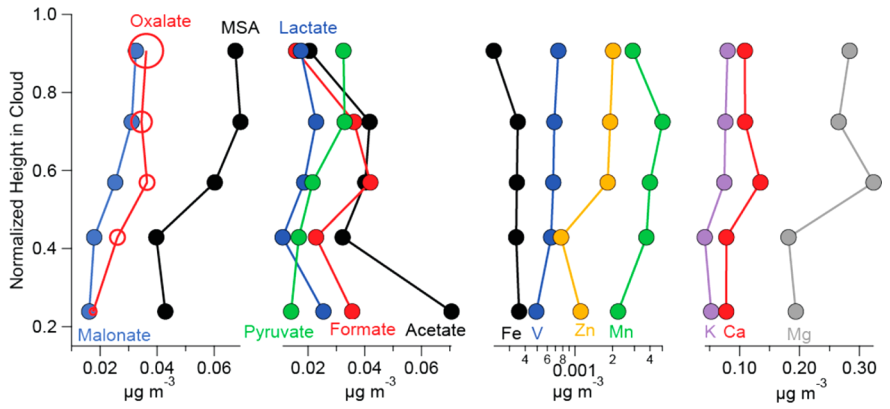

Figure 2. Cumulative average vertical profile of cloudwater constituent concentrations as a function of normalized height in cloud (0 = base, 1 = top). Oxalate marker sizes are proportional to the ratio of oxalate to the sum of all organic acids measured except MSA (range = 0.16−0.37).

precursors in cloud drops; and (ii) organic acids are constituents of supermicrometer and refractory particles not detected below cloud by the C-ToF-AMS. Previous work has shown that acetate and formate accounted for 12% and 33% of total organic carbon in marine stratiform clouds[37] and California radiation fogs,[66] respectively; their uptake from the gas phase might represent a major organic carbon source. Furthermore, the gas/aqueous partitioning of acids might be also biased in cloudwater samples due to different pH values in bulk and size-resolved samples.[67]

The most frequently detected organic acid was MSA (100% of samples) since it is an oxidation product of dimethylsulfide (DMS), which is excreted by phytoplankton in seawater.[68] The next most commonly detected organic acid was oxalate (85% of samples) as it is an end-product of cloud drop processing of organic species. As a result, oxalate exhibits statistically significant correlations (two-tailed student's t-test at 95% confidence) with both DCAs and MCAs. It is a known oxidation product of malonic acid and glyoxylic acid, precursors of which include glyoxal, methylglyoxal, glycolic acid, pyruvic acid, and acetic acid that are all formed from oxidation of many volatile organic compounds (VOCs).[11,12,15,18] Relationships between the organic acids (Table 2) provide support for mechanisms in laboratory and modeling studies (Figure S1 of the Supporting Information (SI)). It is cautioned though that correlations do not necessarily point to a direct pathway between two species. An unexpected result is that oxalate does not exhibit the highest average concentration among the organic acids, since it has previously been shown to be the most abundant organic acid in aerosol particles in the study region[69] and in southeastern Pacific Ocean stratiform cloudwater.[37]

Maleate was detected in 84% of samples and is produced by the oxidation of aromatic hydrocarbons and originates from diesel and gasoline engines.[70] It exhibits a significant correlation with oxalate, MSA, pyruvate, and lactate. For the limited samples glyoxylate was detected in (7 out of 81), oxalate (a product of glyoxylate) and maleate (a precursor to glyoxylate) were simultaneously detected in six. Given the persistence of clouds in the region during E-PEACE, glyoxylate likely was present in more samples but could not be identified due to IC coelution with Cl^-. With the exception of butyric and propionic acids ($n \leq 8$), the MCAs exhibited statistically significant correlations with each other, suggestive of related production routes as compared to the DCAs. The highest MCA concentrations are closest to land suggestive of the influence of fresher continental or coastal emissions (Figure 1). Cumulative vertical concentration profiles of MCAs (mainly acetate and formate) also exhibit differences as compared to

dx.doi.org/10.1021/es4012383 | Environ. Sci. Technol. 2013, 47, 7747−7756

DCAs, which generally increase in concentration with in-cloud altitude (Figure 2). Such results point to a greater contribution of gas-phase sources of MCAs as compared to DCAs.

Among the metals studied, the highest concentrations are accounted for by sodium (Na: 1.93 ± 2.19 μg m^{-3}) and other crustal-derived elements (Si, Mg, Ca, K: individual averages ~0.07−0.26 μg m^{-3}). These components are expectedly the most abundant owing to their associations with sea spray (especially Na) and other potential sources such as dust, continental combustion sources, and ship emissions. A number of other notable trace metals associated with organic acid metal complexation were ubiquitous in the regional cloudwater at lower concentrations (Fe, Zn, Mn, Pb).

Relationships between metals and the water-soluble anions provide insight into common sources. For example, nitrate, nss-sulfate, malonate, Fe, Mn, and V exhibit statistically significant positive correlations with each other (except malonate with Fe and V), with the common source being ship emissions (Table 2). Other work in the region has shown that V is a ship emissions tracer species.[71,72] Cl^- was best correlated with MSA and Ca, owing most likely to wind-driven ocean emissions. Although relating ocean surface emissions solely to wind speed is highly simplified (e.g., 73), it is interesting to note that wind speed exhibited a positive and statistically significant correlation with only Cl^-, Ca, malonate, oxalate, and several crustal constituents not shown in Table 2 (Na, Mg, K). This is suggestive of enhanced ocean surface emissions with higher wind speeds. Other work has indicated that natural marine sources can lead to low molecular weight organic acids, including through secondary production from ocean-emitted vapors, the breakdown of primary biological matter emitted within sea spray aerosols, or the interaction of gaseous DCAs (uptake or heterogeneous reaction) with sea salt particles.[74−76] The closest representation of oxalate and malonate below clouds is m/z 44, which exhibits a statistically significant relationship with only these two organic acids in cloudwater; however, subcloud m/z 44 concentrations in submicrometer particles are not correlated with wind speed. This suggests that faster winds lead to higher concentrations of oxalate and malonate in cloudwater due to direct emissions of coarse particles and gaseous precursors that partition into cloud drops.

3.2. Metal Relationships With Organic Acids. Metal−oxalate interactions are investigated using three case flights that had at least four samples collected in the same general vicinity and at different in-cloud altitudes (Figure 3, Table 3): RF 14 on 27 July, RF 16 on 29 July, RF21 on 5 August. Three-day HYSPLIT[77] back-trajectories corresponding to each sample similarly came south along the coast of the western United States (Figure 3). Of the three flights, specific ones included stronger influences from either ship emissions (RF14/RF16), Si-rich sources (RF16), or wind-driven ocean emissions (RF21). RF14 and RF16 were most influenced by ship emissions as evidenced by high and sustained V concentrations (1.63−2.42 ng m^{-3}) relative to the E-PEACE average and RF21 (0.66 and 0.06−0.29 ng m^{-3}, respectively) (Table 3), and subcloud particle concentrations exceeding 30,000 cm^{-3}. The highest subcloud wind speeds were observed during RF21 (10.2 m s^{-1} versus 2.9−4.9 m s^{-1} for RF14 and RF16), coincident with the highest Cl^- and Na concentrations (Table 3). The higher average Ca and Si levels during RF16 are suggestive of a combination of ship and crustal continental emissions (and not ocean surface emissions), especially since

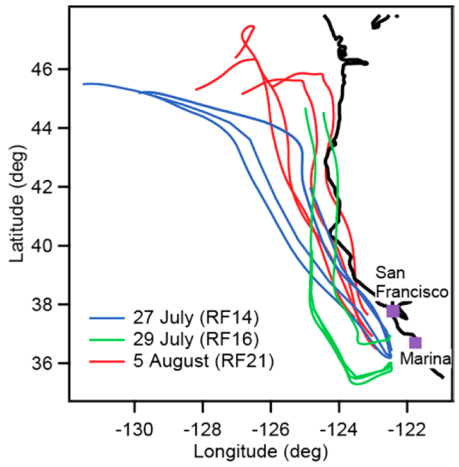

Figure 3. Three day HYSPLIT back-trajectories ending at the point of individual cloudwater samples collected during three case flights.

Cl^- levels were lowest during this flight and back-trajectories were closest to land.

The common link between these flights is that at least one sample in each flight was characterized by significantly lower oxalate concentrations as compared to others collected in the same area. No other organic acid showed a reduction in the low-oxalate samples and this is confirmed by the oxalate:organic acid ratio (denominator includes all organic acids except MSA), which generally increases with altitude in cloud except for the low-oxalate samples. A general increase of this ratio with altitude supports the trend of more aqueous generation of oxalate assuming a simplified trajectory of parcels moving vertically in clouds. The average oxalate:organic acid ratio of the first two samples in RF21 was 18% of that of the final two samples, which is similar to the fractions observed in the other flights between the high metal and adjacent samples (16% in RF14 and 12% in RF16). Potential pH or LWC effects on the reduction of oxalate during these three case flights is ruled out owing to the similar values observed in all samples during each of the individual flights (Table 3). Sampling of widely different air masses is also unlikely as an explanation since other chemical factors (in addition to other organic acids) show no peculiar behavior in the low-oxalate samples: (i) nss-sulfate shows either an increasing (RF14) or decreasing (RF16/RF21) trend as a function of in-cloud altitude without strange behavior in the low-oxalate samples; and (ii) Cl^- shows an expected decreasing trend with altitude since sea salt should be most abundant near cloud base.

The only factor found to exhibit a consistent relationship, either positive or negative, with oxalate in each flight was the concentration of a subset of metal cations: Fe, Mn, K, Na, Mg, Ca. When considering all three flights, the metal showing the strongest anticorrelation was Fe (Table 4); only one of the correlation coefficients is statistically significant at 95% confidence using a two-tailed student's t-test (iron-oxalate for RF21) likely due to nonlinear relationships between the various constituents as will be discussed more below. The observation of oxalate reductions with simultaneous metal enrichment is not specific to any particular altitude based on the three case flights. Metals likely are primarily entrained from the bases of clouds in this region due to ships and wind-driven ocean emissions, but cloud top entrainment cannot be ruled out. The cumulative vertical profile of oxalate during E-PEACE shows an

dx.doi.org/10.1021/es4012383 | Environ. Sci. Technol. 2013, 47, 7747−7756

Table 3. Vertically-Resolved Cloud Water Chemical Data for Three Case Flights[a]

RF	alt (m)/Norm. Cloud height/LWC (g m^{-3})	pH	oxalate: Org Acid	NSS SO_4^{2-}	Cl^-	Na	oxalate	Si	Ca	V	Fe	Mg	K	Mn
14	209/0.15/0.09	3.56	0.08	1.36	1.71	0.97	5.10	8.90	51.68	1.63	4.53	132.24	29.20	0.43
	308/0.51/0.20	3.82	0.14	1.41	0.88	0.54	10.25	0.98	24.14	1.99	3.71	74.54	9.21	0.25
	428/0.79/0.31	4.01	0.17	1.73	0.88	0.46	14.13		23.40	1.95	3.00	66.21	2.58	0.15
	483/0.92/0.38	4.03	0.28	1.72	0.79	0.38	35.90		22.32	2.23	2.97	53.84		0.17
	486/0.93/0.36	3.88	0.05	1.87	0.56	0.25	5.04	0.88	21.15	2.42	3.81	37.34		0.20
16	408/0.41/0.27	3.77	0.28	2.95	0.57	0.36	18.24	107.52	113.95	2.35	18.16	67.94	14.97	2.23
	422/0.56/0.27	3.70	0.44	2.87	0.49	0.32	55.63	92.08	98.16	2.13	14.33	58.03	7.57	1.66
	471/0.73/0.31	3.95	0.06	2.76	0.52	0.56	5.28	165.76	153.27	1.96	21.76	62.73	39.40	1.87
	535/0.96/0.39	3.93	0.61	2.52	0.51	0.31	149.28	57.30	101.56	2.19	13.69	53.85	14.66	1.60
21	282/0.33/0.13	4.14	0.13	1.40	6.34	2.95	4.73	3.44	148.90	0.29	3.28	399.82	94.52	0.54
	420/0.59/0.24	4.52	0.04	1.01	3.51	1.53	2.72		79.73	0.18	3.11	207.00	41.74	0.23
	566/0.84/0.31	4.78	0.49	0.74	2.14	0.87	23.58	13.39	40.54	0.10	1.76	123.40	15.16	0.18
	616/0.93/0.37	5.14	0.48	0.49	1.18	0.46	32.36		19.31	0.06	1.40	63.98		0.05

[a]NSS-sulfate, Na, and Cl^- are in units of μg m^{-3}, whereas all other species are in units of ng m^{-3}. "Norm. Cloud Height" represents the normalized height in cloud where a sample was collected, where 0 and 1 would be the base and top of a cloud, respectively. "Org acid" includes all organic acids in Table 1 except MSA.

Table 4. Correlation (r) between Oxalate and Metal Cation Concentrations in Cloud Water Samples Collected during Three Case Flights (Sample Number Is Shown in Parentheses)

	RF14	RF16	RF21
Fe	−0.74 (5)	−0.81 (4)	−0.99 (4)
Mn	−0.49 (5)	−0.70 (4)	−0.76 (4)
K	−0.98 (3)	−0.47 (4)	−0.70 (3)
Na	−0.33 (5)	−0.65 (4)	−0.81 (4)
Mg	−0.34 (5)	−0.86 (4)	−0.81 (4)
Ca	−0.39 (5)	−0.64 (4)	−0.84 (4)
Si	−0.48 (3)	0.86 (4)	
V	0.30 (5)	0.18 (4)	−0.88 (4)

increase in oxalate from cloud base to the midpoint of clouds, above which it is stable in concentration at approximately 35 ng m^{-3} (Figure 2). Iron concentrations increase as a function of in-cloud altitude (3−5 ng m^{-3}) except for the very top (2 ng m^{-3}). These concentrations are lower than those measured in southeastern Pacific Ocean stratiform cloudwater (average Fe = 17 ng m^{-3}[337]). Other metal cations exhibit varying vertical profiles, reflecting their different sources. The oxalate:organic ratio increases gradually with altitude presumably due to a combination of increased aqueous processing time and the ability of metal effects to occur at any altitude in clouds, based on the analysis of the three case flights.

A backward stepwise linear regression was performed to identify the best predictors of oxalate concentrations using available chemical measurements. The analysis used 13 species (oxalate, MSA, Cl^-, NO_3^-, nss-sulfate, Na, Mg, Ca, V, Mn, Fe, Cu, Zn). The resulting relationship is obtained in mass concentration units (r^2 = 0.58, n = 52):

$$\text{oxalate} = 0.002 + 0.071[NO_3^-] + 0.875[Ca] - 0.036[Na] - 31.586[V] - 8.339[Fe] + 0.668[Cu] + 4.451[Zn]$$

The predictor with the highest statistical significance was NO_3^- followed in order by Fe, Zn, V, Ca, Na, and Cu. While the case studies highlight the effect of Fe in individual flights, the cumulative data set also shows an inverse relationship further providing motivation to improve understanding of this sink for oxalate.

3.3. Model Simulations. In order to understand the negative correlation between oxalate and iron, we use a multiphase chemistry box model that includes a previously applied chemical mechanism[12] and in addition the formation and photolysis of iron hydroxo and oxalato complexes and Fe(II)/(III) redox cycling by HO_x radicals and H_2O_2. (Details

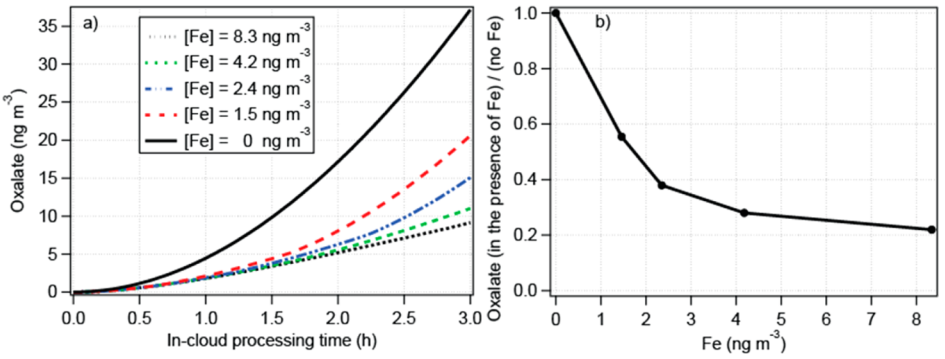

Figure 4. (a) Predicted oxalate concentrations as a function of cloud-processing time for different concentrations of total dissolved iron. (b) Ratio of predicted oxalate concentrations from simulations with and without iron as a function of total iron concentration dissolved in cloudwater. Box model conditions are summarized in the SI.

dx.doi.org/10.1021/es4012383 | Environ. Sci. Technol. 2013, 47, 7747−7756

of the multiphase mechanism are given in the SI.) Model simulations are performed for a constant LWC (0.3 g m^{-3}) and a drop size distribution covering a size range of ~8−30 μm over three hours, which might be a reasonable estimate of total cloud processing times during multiple cloud cycles along the trajectories in Figure 3. Photolysis rates are assumed constant during the simulation time. These rates are adjusted for the geographical location and date; we do not consider any effects of clouds on photolysis rates that could lead to an overestimate in the interstitial spaces of optically thick clouds or their underestimate in the interstitial spaces in optically thin regions.[78,79] The current data set did not provide size-resolved data; however, in agreement with previous measurements in cloud and fogwater[56] we assume decreasing iron and proton concentrations with increasing drop size (details in the SI). Since the purpose of the model studies is to highlight the impact of Fe on oxalate levels, the only difference between the various simulations are the iron levels.

In Figure 4a, predicted overall oxalate concentrations are compared between model simulations without and with Fe. The model results suggest that even small amounts of dissolved Fe lead to significantly lower oxalate concentrations. Analysis of the contributions by the different drop sizes reveals that oxalate is predominantly formed in the most abundant droplet sizes (SI Figures S2a and S2b). Predicted size-resolved aqueous-phase concentrations are in agreement with the observed enhancement of oxalate concentrations with decreasing droplet size.[67]

The predicted decrease in oxalate as a function of total Fe concentration does not linearly scale with Fe (Figure 4b). The predicted oxalate concentration as a function of Fe nearly levels off for Fe concentrations above ~3 ng m^{-3} (for the model conditions here) and overall predicted oxalate levels above such Fe concentrations are about 15% of those that are predicted without consideration of iron redox cycling reactions (~40 ng m^{-3} versus ~7 ng m^{-3}, Figure 4a). The nonlinear impact of Fe on oxalate might be explained by the fact that most Fe is present as Fe(II) during daytime conditions. Thus, only a minor Fe fraction (~10%) is in the form of Fe(III), which is needed to form oxalato complexes. While qualitatively our results agree with observed Fe(II)/Fe(III) ratios greater than unity at other locations,[80−82] the efficient depletion of Fe(III) in our model might be an overestimate since it has been shown that other Fe(III)−organo complexes might be more stable.[38] The trends in the model results clearly show that the photolysis of the Fe(III)−oxalato complexes is an efficient sink for oxalate and has to be included in models that use oxalate as a tracer of cloud-processing and SOA formation in the aqueous phase.

3.4. IMPLICATIONS OF OXALATE-METAL INTERACTIONS IN STUDY REGION

Oxalic acid can form metal complexes in the marine boundary layer due to the ubiquity of metals in directly emitted particle types (e.g., sea salt, dust, fly ash), the ubiquity of oxalate in aerosol particles in the study region,[26,36,69] and the favorable aqueous-phase medium provided by cloud drops to promote efficient complexation between metal and oxalate ions.[83] While we only considered complexation of iron by oxalate, other organic ligands (acids, humic like substances) might also form iron complexes. Thus our model calculations can be regarded as an upper limit of Fe(III) impact on oxalate levels.

Enhanced metal levels (e.g., Cu, Mn, Fe) also impact HO_x levels in the aqueous phase in a complex manner and thus might affect the oxidation capacity of the aqueous phase in additional ways. That the three case events occurred in different pollution regimes with varying ratios between metals shows that oxalate-metal interactions can occur in a variety of conditions experienced in this study region and occur frequently due to the probable influence of either marine, ship, or continental emissions at a given time. The observation of an inverse relationship between metal and oxalate concentrations has major implications for predictive capabilities of oxalate formation in the atmosphere in light of recent studies neglecting this sink.[84] The E-PEACE measurements, together with box model simulations, can explain the significant overestimate of predicted oxalate levels versus in-cloud measurements in the same study region almost a decade ago.[26]

■ ASSOCIATED CONTENT

Supporting Information

Two additional figures are provided to summarize documented organic acid chemical mechanisms and more results related to Section 3.3. Details related to the model used for Section 3.3 are provided. This material is available free of charge via the Internet at http://pubs.acs.org.

■ AUTHOR INFORMATION

Corresponding Author

*Phone: (520) 626-5858; fax: (520) 621-6048; e-mail: armin@email.arizona.edu.

Present Address

A.S.: Department of Chemical and Environmental Engineering, University of Arizona, PO BOX 210011, Tucson, Arizona, 85721

Notes

The authors declare no competing financial interest.

■ ACKNOWLEDGMENTS

This work was funded by ONR grants N00014-10-1-0811, N00014-11-1-0783, and N00014-10-1-0200. We acknowledge Dean Hegg for providing the cloudwater collector. We gratefully acknowledge the NOAA Air Resources Laboratory (ARL) for the provision of the HYSPLIT transport and dispersion model and READY website (http://ready.arl.noaa.gov) used in this publication. BE acknowledges support from NOAA's Climate Goal.

■ REFERENCES

(1) McKeen, S.; Chung, S. H.; Wilczak, J.; Grell, G.; Djalalova, I.; Peckham, S.; Gong, W.; Bouchet, V.; Moffet, R.; Tang, Y.; Carmichael, G. R.; Mathur, R.; Yu, S. Evaluation of several $PM_{2.5}$ forecast models using data collected during the ICARTT/NEAQS 2004 field study. *J. Geophys. Res.* **2007**, *112*, D10S20 DOI: 10.1029/2006JD007608.

(2) Ervens, B.; Volkamer, R. Glyoxal processing by aerosol multiphase chemistry: Towards a kinetic modeling framework of secondary organic aerosol formation in aqueous particles. *Atmos. Chem. Phys.* **2010**, *10*, 8219−8244, DOI: 10.5194/acp-10-8219-2010.

(3) Tan, Y.; Lim, Y. B.; Altieri, K. E.; Seitzinger, S. P.; Turpin, B. J. Mechanisms leading to oligomers and SOA through aqueous photooxidation: Insights from OH radical oxidation of acetic acid. *Atmos. Chem. Phys.* **2012**, *12*, 801−813.

(4) de Gouw, J. A.; Middlebrook, A. M.; Warneke, C.; Goldan, P. D.; Kuster, W. C.; Roberts, J. M.; Fehsenfeld, F. C.; Worsnop, D. R.; Canagaratna, M. R.; Pszenny, A. A. P.; Keene, W. C.; Marchewka, M.; Bertman, S. B.; Bates, T. S. Budget of organic carbon in a polluted atmosphere: Results from the New England Air Quality Study in 2002. *J. Geophys. Res.* **2005**, *110*, D16305 DOI: 10.1029/2004JD005623.

(5) Heald, C. L.; Jacob, D. J.; Park, R. J.; Russell, L. M.; Huebert, B. J.; Seinfeld, J. H.; Liao, H.; Weber, R. J. A large organic aerosol source in the free troposphere missing from current models. *Geophys. Res. Lett.* **2005**, *32*, L18809 DOI: 10.1029/2005GL023831.
(6) Volkamer, R.; Jimenez, J. L.; SanMartini, F.; Dzepina, K.; Zhang, Q.; Salcedo, D.; Molina, L. T.; Worsnop, D. R.; Molina, M. J. Secondary organic aerosol formation from anthropogenic air pollution: Rapid and higher than expected. *Geophys. Res. Lett.* **2006**, *33*, L17811 DOI: 10.1029/2006GL026899.
(7) Blando, J. D.; Turpin, B. J. Secondary organic aerosol formation in cloud and fog droplets: A literature evaluation of plausibility. *Atmos. Environ.* **2000**, *34*, 1623−1632.
(8) Heald, C. L.; Jacob, D. J.; Turquety, S.; Hudman, R. C.; Weber, R. J.; Sullivan, A. P.; Peltier, R. E.; Atlas, E. L.; de Gouw, J. A.; Warneke, C.; Holloway, J. S.; Neuman, J. A.; Flocke, F. M.; Seinfeld, J. H. Concentrations and sources of organic carbon aerosols in the free troposphere over North America. *J. Geophys. Res.* **2006**, *111*, D23S47 DOI: 10.1029/2006JD007705.
(9) Chen, J.; Griffin, R. J.; Grini, A.; Tulet, P. Modeling secondary organic aerosol formation through cloud processing of organic compounds. *Atmos. Chem. Phys.* **2007**, *7*, 5343−5355.
(10) Carlton, A. G.; Turpin, B. J.; Altieri, K.; Seitzinger, S.; Mathur, R.; Roselle, S. CMAQ model performance enhanced when in-cloud secondary organic aerosol is included: Comparisons of organic carbon predictions with measurements. *Environ. Sci. Technol.* **2008**, *42*, 8798−8802.
(11) Warneck, P. In-cloud chemistry opens pathway to the formation of oxalic acid in the marine atmosphere. *Atmos. Environ.* **2003**, *37*, 2423−2427.
(12) Ervens, B.; Feingold, G.; Frost, G. J.; Kreidenweis, S. M. A modeling study of aqueous production of dicarboxylic acids: 1. Chemical pathways and speciated organic mass production. *J. Geophys. Res.* **2004**, *109*, D15205 DOI: 10.1029/2003JD004387.
(13) Ervens, B.; Carlton, A. G.; Turpin, B. J.; Altieri, K. E.; Kreidenweis, S. M.; Feingold, G. Secondary organic aerosol yields from cloud-processing of isoprene oxidation products. *Geophys. Res. Lett.* **2008**, *35*, L02816 DOI: 10.1029/2007GL031828.
(14) Gelencser, A.; Varga, Z. Evaluation of the atmospheric significance of multiphase reactions in atmospheric secondary organic aerosol formation. *Atmos. Chem. Phys.* **2005**, *5*, 2823−2831.
(15) Lim, H. J.; Carlton, A. G.; Turpin, B. J. Isoprene forms secondary organic aerosol through cloud processing: Model simulations. *Environ. Sci. Technol.* **2005**, *39*, 4441−4446.
(16) Huang, X. H. H.; Ip, H. S. S.; Yu, J. Z. Secondary organic aerosol formation from ethylene in the urban atmosphere of Hong Kong: A multiphase chemical modeling study. *J. Geophys. Res.* **2011**, *116*, D03206 DOI: 10.1029/2010JD014121.
(17) Liggio, J.; Li, S. M.; McLaren, R. Heterogeneous reactions of glyoxal on particulate matter: Identification of acetals and sulfate esters. *Environ. Sci. Technol.* **2005**, *39*, 1532−1541.
(18) Carlton, A. G.; Turpin, B. J.; Lim, H. J.; Altieri, K. E.; Seitzinger, S. Link between isoprene and secondary organic aerosol (SOA): Pyruvic acid oxidation yields low volatility organic acids in clouds. *Geophys. Res. Lett.* **2006**, *33*, L06822 DOI: 10.1029/2005GL025374.
(19) Carlton, A. G.; Turpin, B. J.; Altieri, K. E.; Seitzinger, S.; Reff, A.; Lim, H. J.; Ervens, B. Atmospheric oxalic acid and SOA production from glyoxal: Results of aqueous photooxidation experiments. *Atmos. Environ.* **2007**, *41*, 7588−7602.
(20) Altieri, K. E.; Seitzinger, S. P.; Carlton, A. G.; Turpin, B. J.; Klein, G. C.; Marshall, A. G. Oligomers formed through in−cloud methylglyoxal reactions: Chemical composition, properties, and mechanisms investigated by ultra−high resolution FT−ICR mass spectrometry. *Atmos. Environ.* **2008**, *42*, 1476−1490.
(21) Corrigan, A. L.; Hanley, S. W.; Haan, D. O. Uptake of glyoxal by organic and inorganic aerosol. *Environ. Sci. Technol.* **2008**, *42*, 4428−4433.
(22) Perri, M. J.; Seitzinger, S.; Turpin, B. J. Secondary organic aerosol production from aqueous photooxidation of glycolaldehyde: Laboratory experiments. *Atmos. Environ.* **2009**, *43*, 1487−1497.
(23) El Haddad, I.; Yao Liu, Nieto-Gligorovski, L.; Michaud, V.; Temime-Roussel, B.; Quivet, E.; Marchand, N.; Sellegri, K.; Monod, A. In-cloud processes of methacrolein under simulated conditions − Part 2: Formation of secondary organic aerosol. *Atmos. Chem. Phys.* **2009**, *9*, 5107−5117, DOI: 10.5194/acp-9-5107-2009.
(24) Sun, Y. L.; Zhang, Q.; Anastasio, C.; Sun, J. Insights into secondary organic aerosol formed via aqueous-phase reactions of phenolic compounds based on high resolution mass spectrometry. *Atmos. Chem. Phys.* **2010**, *10*, 4809−4822, DOI: 10.5194/acp-10-4809-2010.
(25) Volkamer, R.; Ziemann, P. J.; Molina, M. J. Secondary organic aerosol formation from acetylene (C_2H_2): Seed effect on SOA yields due to organic photochemistry in the aerosol aqueous phase. *Atmos. Chem. Phys.* **2009**, *9*, 1907−1928.
(26) Crahan, K. K.; Hegg, D.; Covert, D. S.; Jonsson, H. An exploration of aqueous oxalic acid production in the coastal marine atmosphere. *Atmos. Environ.* **2004**, *38*, 3757−3764.
(27) Yu, J. Z.; Huang, X. F.; Xu, J.; Hu, M. When aerosol sulfate goes up, so does oxalate: Implication for the formation mechanisms of oxalate. *Environ. Sci. Technol.* **2005**, *39*, 128−133.
(28) Sorooshian, A.; Varutbangkul, V.; Brechtel, F. J.; Ervens, B.; Feingold, G.; Bahreini, R.; Murphy, S. M.; Holloway, J. S.; Atlas, E. L.; Buzorius, G.; Jonsson, H.; Flagan, R. C.; Seinfeld, J. H. Oxalic acid in clear and cloudy atmospheres: Analysis of data from International Consortium for Atmospheric Research on Transport and Transformation 2004. *J. Geophys. Res.* **2006**, *111*, D23S45 DOI: 10.1029/2005JD006880.
(29) Hennigan, C. J.; Bergin, M. H.; Dibb, J. E.; Weber, R. J. Enhanced secondary organic aerosol formation due to water uptake by fine particles. *Geophys. Res. Lett.* **2008**, *35*, L18801 DOI: 10.1029/2008gl035046.
(30) Hennigan, C. J.; Bergin, M. H.; Russell, A. G.; Nenes, A.; Weber, R. J. Gas/particle partitioning of water-soluble organic aerosol in Atlanta. *Atmos. Chem. Phys.* **2009**, *9*, 3613−3628.
(31) Miyazaki, Y.; Aggarwal, S. G.; Singh, K.; Gupta, P. K.; Kawamura, K. Dicarboxylic acids and water-soluble organic carbon in aerosols in New Delhi, India, in winter: Characteristics and formation processes. *J. Geophys. Res.* **2009**, *114*, D19206 DOI: 10.1029/2009jd011790.
(32) Duong, H. T.; Sorooshian, A.; Craven, J. S.; Hersey, S. P.; Metcalf, A. R.; Zhang, X.; Weber, R. J.; Jonsson, H.; Flagan, R. C.; Seinfeld, J. H. Water−soluble organic aerosol in the Los Angeles Basin and outflow regions: Airborne and ground measurements during the 2010 CalNex field campaign. *J. Geophys. Res.* **2011**, *116*, D00V04 DOI: 10.1029/2011JD016674.
(33) Kaul, D. S.; Gupta, T.; Tripathi, S. N.; Tare, V.; Collett, J. L. Secondary organic aerosol: A comparison between foggy and nonfoggy days. *Environ. Sci. Technol.* **2011**, *45*, 7307−7313, DOI: 10.1021/es201081d.
(34) Wonaschütz, A.; Sorooshian, A.; Ervens, B.; Chuang, P. Y.; Feingold, G.; Murphy, S. M.; deGouw, J.; Warneke, C.; Jonsson, H. H. Aerosol and gas re-distribution by shallow cumulus clouds: An investigation using airborne measurements. *J. Geophys. Res.* **2012**, *117*, D17202 DOI: 10.1029/2012JD018089.
(35) Sorooshian, A.; Ng, N. L.; Chan, A. W. H.; Feingold, G.; Flagan, R. C.; Seinfeld, J. H. Particulate organic acids and overall water-soluble aerosol composition measurements from the 2006 Gulf of Mexico Atmospheric Composition and Climate Study (GoMACCS). *J. Geophys. Res.* **2007**, *112*, D13201 DOI: 10.1029/2007JD008537.
(36) Sorooshian, A.; Murphy, S. M.; Hersey, S.; Bahreini, R.; Jonsson, H.; Flagan, R. C.; Seinfeld, J. H. Constraining the contribution of organic acids and AMS m/z 44 to the organic aerosol budget: On the importance of meteorology, aerosol hygroscopicity, and region. *Geophys. Res. Lett.* **2010**, *37*, L21807 DOI: 10.1029/2010GL044951.
(37) Benedict, K. B.; Lee, T.; Collett, J. L. Cloud water composition over the southeastern Pacific Ocean during the VOCALS regional experiment. *Atmos. Environ.* **2012**, *46*, 104−114.

(38) Paris, R.; Desboeufs, K. V. Effect of atmospheric organic complexation on iron-bearing dust solubility. *Atmos. Chem. Phys. Discuss.* **2013**, *13* (2), 3179−3202.
(39) Kawamura, K.; Kasukabe, H.; Barrie, L. A. Secondary formation of water−soluble organic acids and a−dicarbonyls and their contributions to total carbon and water−soluble organic carbon: Photochemical aging of organic aerosols in the Arctic spring. *J. Geophys. Res.* **2010**, *115*, D21306 DOI: 10.1029/2010JD014299.
(40) Durkee, P. A.; Noone, K. J.; Bluth, R. T. The Monterey Area Ship Track Experiment. *J. Atmos. Sci.* **2000**, *57*, 2523−2541.
(41) Noone, K. J.; Johnson, D. W.; Taylor, J. P.; Ferek, R. J.; Garrett, T.; Hobbs, P. V.; Durkee, P. A.; Nielsen, K.; Ostrom, E.; O'Dowd, C.; Smith, M. H.; Russell, L. M.; Flagan, R. C.; Seinfeld, J. H.; De Bock, L.; Van Grieken, R. E.; Hudson, J. G.; Brooks, I.; Gasparovic, R. F.; Pockalny, R. A. A case study of ship track formation in a polluted marine boundary layer. *J. Atmos. Sci.* **2000**, *57*, 2748−2764.
(42) Stevens, B.; Lenschow, D. H.; Vali, G.; Gerber, H.; Bandy, A.; Blomquist, B.; Brenguier, J. L.; Bretherton, C. S.; Burnet, F.; Campos, T.; Chai, S.; Faloona, I.; Friesen, D.; Haimov, S.; Laursen, K.; Lilly, D. K.; Loehrer, S. M.; Malinowski, S. P.; Morley, B.; Petters, M. D.; Rogers, D. C.; Russell, L.; Savic-Jovac, V.; Snider, J. R.; Straub, D.; Szumowski, M. J.; Takagi, H.; Thornton, D. C.; Tschudi, M.; Twohy, C.; Wetzel, M.; van Zanten, M. C. Dynamics and chemistry of marine stratocumulus—DYCOMS-II. *Bull. Am. Meteorol. Soc.* **2003**, *84*, 579−593.
(43) Lu, M. L.; Conant, W. C.; Jonsson, H. H.; Varutbangkul, V.; Flagan, R. C.; Seinfeld, J. H. The marine stratus/stratocumulus experiment (MASE): Aerosol-cloud relationships in marine stratocumulus. *J. Geophys. Res.* **2007**, *112*, DOI: 10.1029/2006jd007985.
(44) Lu, M. L.; Sorooshian, A.; Jonsson, H. H.; Feingold, G.; Flagan, R. C.; Seinfeld, J. H. Marine stratocumulus aerosol-cloud relationships in the MASE-II experiment: Precipitation susceptibility in eastern pacific marine stratocumulus. *J. Geophys. Res.* **2009**, *114*, DOI: 10.1029/2009jd012774.
(45) Hegg, D. A.; Gao, S.; Jonsson, H. Measurements of selected dicarboxylic acids in marine cloud water. *Atmos. Res.* **2002**, *62*, 1−10.
(46) Straub, D. J.; Lee, T.; Collett, J. L. Chemical composition of marine stratocumulus clouds over the eastern Pacific Ocean. *J. Geophys. Res.* **2007**, *112*, D04307 DOI: 10.1029/2006JD007439.
(47) Hegg, D. A.; Covert, D.; Jonsson, H.; Woods, R. Differentiating natural and anthropogenic cloud condensation nuclei in the California coastal zone. *Tellus B.* **2009**, *61*, 669−676.
(48) Russell, L. M.; Sorooshian, A.; Seinfeld, J. H.; Albrecht, B. A.; Nenes, A.; Ahlm, L.; Chen, Y.-C.; Coggon, M. M.; Craven, J. S.; Flagan, R. C.; Frossard, A. A.; Jonsson, H.; Jung, E.; Lin, J. J.; Metcalf, A. R.; Modini, R.; Mülmenstädt, J.; Roberts, G. C.; Shingler, T.; Song, S.; Wang, Z.; Wonaschütz, A. Eastern Pacific Emitted Aerosol Cloud Experiment (E-PEACE). *Bull. Am. Meteorol. Soc.* **2013**, *94*, 709−729, DOI: http://dx.doi.org/10.1175/BAMS-D-12-00015.1.
(49) Coggon, M. M.; Sorooshian, A.; Wang, Z.; Metcalf, A. R.; Frossard, A. A.; Lin, J. J.; Craven, J. S.; Nenes, A.; Jonsson, H. H.; Russell, L. M.; Flagan, R. C.; Seinfeld, J. H. Ship impacts on the marine atmosphere: Insights into the contribution of shipping emissions to the properties of marine aerosol and clouds. *Atmos. Chem. Phys.* **2012**, *12*, 8439−8458.
(50) Wonaschütz, A.; Coggon, M.; Sorooshian, A.; Modini, R.; Frossard, A. A.; Ahlm, L.; Mülmenstädt, J.; Roberts, G. C.; Russell, L. M.; Dey, S.; Brechtel, F. J.; Seinfeld, J. H. Hygroscopic properties of organic aerosol particles emitted in the marine atmosphere. *Atmos. Chem. Phys. Discuss.* **2013**, *13*, 11919−11969, DOI: 10.5194/acpd-13-11919-2013.
(51) Chen, Y.-C.; Christensen, M. W.; Xue, L.; Sorooshian, A.; Stephens, G. L.; Rasmussen, R. M.; Seinfeld, J. H. Occurrence of lower cloud albedo in ship tracks. *Atmos. Chem. Phys.* **2012**, *12*, 8223−8235.
(52) Hegg, D. A.; Hobbs, P. V. Sulfate and nitrate chemistry in marine cumuliform clouds. *Atmos. Environ.* **1986**, *20*, 901−909.
(53) Hegg, D. A.; Hobbs, P. V. *Studies of the Mechanisms and Rate with Which Nitrogen Species Are Incorporated into Cloud Water and Precipitation*, . Second Annual Report on Project CAPA-21-80 to the Coordinating Research Council, 1986.
(54) Millet, M.; Sanusi, A.; Wortham, H. Chemical composition of fogwater in an urban area: Strasbourg (France). *Environ. Pollut.* **1996**, *94* (3), 345−354.
(55) Bator, A.; Collett, J. L. Cloud chemistry varies with drop size. *J. Geophys. Res.* **1997**, *102* (D23), 28071−28078.
(56) Rao, X.; Collett, J. L. The drop size-dependence of iron and manganese concentrations in clouds and fogs: Implications for sulfate production. *J. Atmos. Chem.* **1998**, *30* (2), 273−289.
(57) Herckes, P.; Lee, T.; Trenary, L.; Kang, G. G.; Chang, H.; Collett, J. L. Organic matter in Central California radiation fogs. *Environ. Sci. Technol.* **2002**, *36* (22), 4777−4782.
(58) Seinfeld, J. H.; Pandis, S. N. *Atmospheric Chemistry and Physics*, 2nd ed.; Wiley-Interscience: New York, 2006.
(59) Hegg, D. A.; Covert, D. S.; Jonsson, H.; Covert, P. A. Determination of the transmission efficiency of an aircraft aerosol inlet. *Aerosol Sci. Technol.* **2005**, *39*, 966−971.
(60) Shingler, T.; Dey, S.; Sorooshian, A.; Brechtel, F. J.; Wang, Z.; Metcalf, A. R.; Coggon, M.; Mulmenstadt, J.; Russell, L. M.; Jonsson, H. H.; Seinfeld, J. H. Characterization and airborne deployment of a new counterflow virtual impactor. *Atmos. Meas. Tech.* **2012**, *5*, 1515−1541.
(61) Drewnick, F.; Hings, S. S.; DeCarlo, P.; Jayne, J. T.; Gonin, M.; Fuhrer, K.; Weimer, S.; Jimenez, J. L.; Demerjian, K. L.; Borrmann, S.; Worsnop, D. R. A new time-of-flight aerosol mass spectrometer (TOF-AMS)—Instrument description and first field deployment. *Aerosol Sci. Technol.* **2005**, *39*, 637−658.
(62) McLafferty, F. W.; Turecek, F. *Interpretation of Mass Spectra*, 4th ed.; University Science Books: Mill Valley, CA, 1993.
(63) Zhang, Q.; Alfarra, M. R.; Worsnop, D. R.; Allan, J. D.; Coe, H.; Canagaratna, M. R.; Jimenez, J. L. Deconvolution and quantification of hydrocarbon-like and oxygenated organic aerosols based on aerosol mass spectrometry. *Environ. Sci. Technol.* **2005**, *39*, 4938−4952, DOI: 10.1021/Es048568l.
(64) Gerber, H.; Arends, B. G.; Ackerman, A. S. New microphysics sensor for aircraft use. *Atmos. Res.* **1994**, *31*, 235−252.
(65) Baumgardner, D.; Jonsson, H.; Dawson, W.; O'Connor, D.; Newton, R. The cloud, aerosol and precipitation spectrometer: A new instrument for cloud investigations. *Atmos. Res.* **2001**, *59−60*, 251−264.
(66) Collett, J. L.; Herckes, P.; Youngster, S.; Lee, T. Processing of atmospheric organic matter by California radiation fogs. *Atmos. Res.* **2008**, *87* (3−4), 232−241.
(67) Ervens, B.; Herckes, P.; Feingold, G.; Lee, T.; Collett, J. L.; Kreidenweis, S. M. On the drop-size dependence of organic acid and formaldehyde concentrations in fog. *J. Atmos. Chem.* **2003**, *46* (3), 239−269.
(68) Charlson, R. J.; Lovelock, J. E.; Andreae, M. O.; Warren, S. G. Oceanic phytoplankton, atmospheric sulphur, cloud albedo and climate. *Nature* **1987**, *326*, 655−661.
(69) Sorooshian, A.; Lu, M.-L.; Brechtel, F. J.; Jonsson, H.; Feingold, G.; Flagan, R. C.; Seinfeld, J. H. On the source of organic acid aerosol layers above clouds. *Environ. Sci. Technol.* **2007**, *41*, 4647−4654.
(70) Rogge, W. F.; Mazurek, M. A.; Hildemann, L. M.; Cass, G. R.; Simoneit, B. R. T. Quantification of urban organic aerosols at a molecular level—Identification, abundance and seasonal variation. *Atmos. Environ.* **1993**, *27*, 1309−1330.
(71) Murphy, S. M.; Agrawal, H.; Sorooshian, A.; Padro, L. T.; Gates, H.; Hersey, S.; Welch, W. A.; Jung, H.; Miller, J. W.; Cocker, D. R., III; Nenes, A.; Jonsson, H. H.; Flagan, R. C.; Seinfeld, J. H. Comprehensive simultaneous shipboard and airborne characterization of exhaust from a modern container ship at sea. *Environ. Sci. Technol.* **2009**, *43*, 4626−4640.
(72) Ault, A. P.; Gaston, C. J.; Wang, Y.; Dominguez, G.; Thiemens, M. H.; Prather, K. A. Characterization of the single particle mixing state of individual ship plume events measured at the port of Los Angeles. *Environ. Sci. Technol.* **2010**, *44*, 1954−1961.

(73) Jaegle, L.; Quinn, P. K.; Bates, T. S.; Alexander, B.; Lin, J. T. Global distribution of sea salt aerosols: New constraints from in situ and remote sensing observations. *Atmos. Chem. Phys.* **2011**, *11* (7), 3137−3157.
(74) Mochida, M.; Umemoto, N.; Kawamura, K.; Uematsu, M. Bimodal size distribution of C2−C4 dicarboxylic acids in the marine aerosols. *Geophys. Res. Lett.* **2003**, *30* (13), 1672 DOI: 10.1029/2003GL017451.
(75) Mochida, M.; Umemoto, N.; Kawamura, K.; Lim, H. −J.; Turpin, B. J. Bimodal size distributions of various organic acids and fatty acids in the marine atmosphere: Influence of anthropogenic aerosols, Asian dusts, and sea spray off the coast of East Asia. *J. Geophys. Res.* **2007**, *112*, D15209 DOI: 10.1029/2006JD007773.
(76) Rinaldi, M.; Decesari, S.; Carbone, C.; Finessi, E.; Fuzzi, S.; Ceburnis, D.; O'Dowd, C. D.; Sciare, J.; Burrows, J. P.; Vrekoussis, M.; Ervens, B.; Tsigaridis, K.; Facchini, M. C. Evidence of a natural marine source of oxalic acid and a possible link to glyoxal. *J. Geophys. Res.* **2011**, *116*, D16204 DOI: 10.1029/2011JD015659.
(77) Draxler, R. R.; Rolph, G. D. *HYSPLIT (HYbrid Single-Particle Lagrangian Integrated Trajectory) Model*, access via NOAA ARL READY Website (http://ready.arl.noaa.gov/HYSPLIT.php); NOAA Air Resources Laboratory, Silver Spring, MD, 2012.
(78) Mayer, B.; Kylling, A.; Madronich, S.; Seckmeyer, G. Enhanced absorption of UV radiation due to multiple scattering in clouds: Experimental evidence and theoretical explanation. *J. Geophys. Res.* **1998**, *103* (D23), 31241−31254, DOI: 10.1029/98jd02676.
(79) Tie, X.; Madronich, S.; Walters, S.; Zhang, R.; Rasch, P.; Collins, W. Effects of clouds on photolysis and oxidants in the troposphere. *J. Geophys. Res.*, **2003**, *108*, D20, DOI 10.1029/2003JD003659.
(80) Behra, P.; Sigg, L. Evidence for redox cycling of iron in atmospheric water droplets. *Nature* **1990**, *344* (6265), 419−421.
(81) Erel, Y.; Pehkonen, S. O.; Hoffmann, M. R. Redox chemistry of iron in fog and stratus clouds. *J. Geophys. Res.* **1993**, *98* (D10), 18423−18434.
(82) Kieber, R. J.; Williams, K.; Willey, J. D.; Skrabal, S.; Avery, G. B. Iron speciation in coastal rainwater: Concentration and deposition to seawater. *Mar. Chem.* **2001**, *73* (2), 83−95.
(83) Furukawa, T.; Takahashi, Y. Oxalate metal complexes in aerosol particles: Implications for the hygroscopicity of oxalate-containing particles. *Atmos. Chem. Phys.* **2011**, *11* (9), 4289−4301.
(84) Myriokefalitakis, S.; Tsigaridis, K.; Mihalopoulos, N.; Sciare, J.; Nenes, A.; Kawamura, K.; Segers, A.; Kanakidou, M. In-cloud oxalate formation in the global troposphere: A 3-D modeling study. *Atmos. Chem. Phys.* **2011**, *11* (12), 5761−5782.